Brain Stimulation 18 (2025) 131–137

Contents lists available at ScienceDirect

Brain Stimulation

journal homepage: www.journals.elsevier.com/brain-stimulation

Techniques and Methods

MRI free targeting of deep brain structures based on facial landmarks

Thomas S. Riis *, Seth Lunt, Jan Kubanek

Department of Biomedical Engineering, 36 S Wasatch Dr, 84112, Salt Lake City, UT, United States

ARTICLE INFO

Keywords:
Neuronavigation
Deep brain
Neuromodulation

ABSTRACT

Emerging neurostimulation methods aim to selectively modulate deep brain structures. Guiding these therapies has presented a substantial challenge, since imaging modalities such as MRI limit the spectrum of beneficiaries. In this study, we assess the guidance accuracy of a neuronavigation method that does not require taking MRI scans. The method is based on clearly identifiable anatomical landmarks of each subject's face. We compared this technique to the ideal case, MRI-based nonlinear brain registration, and evaluated the accuracy of both methods across ten targets located in deep brain structures: 7 targets in the anterior cingulate cortex as well as the anterior commissure and posterior commissure. Compared with the ideal case, the average localization error of the MRI-free method was 5.75 ± 2.98 mm (mean ± sd). These findings suggest that this method may provide sufficient compromise between practicality and the accuracy of targeting deep brain structures.

1. Introduction

Selective engagement of deep brain structures with modern neuromodulation techniques has required appropriate guidance tools. Existing neuronavigation approaches, based on anatomical landmarks, adhesive fiducials, bone-implanted fiducials, or surface matching [1,2] are based on structural magnetic resonance imaging (MRI) [3,4]. However, MRI presents a limitation to a broad adoption, as many subjects do not have the means to travel to specific MRI facilities and pay the relatively high fees. Other subjects, with claustrophobia or implanted devices, are left out entirely.

Instead of collecting subject-specific MRIs, it is possible to use a template brain, such as the MNI152 [5]. Several studies have quantified targeting accuracy between this template MRI registration and the subject-specific MRI registration for targets placed on the scalp [6–8]. For such targets, template-based registration results in targeting errors generally less than 5 mm. Carducci et al. [6] showed an average error of 4.69 ± 2.21 across the 10–20 EEG locations on the scalp with a max error of 11.53, and Fleishchmann et al. [7] showed an error of 4.79 ± 2.62 with a max error of 9.62. This relatively small registration error offers a promising solution for neuromodulation therapies like transcranial magnetic stimulation (TMS) that engage superficial regions of the brain at relatively broad extent [9].

However, it has been unclear how accurate these methods might be for selective targeting of deep brain structures using emerging approaches such as transcranial focused ultrasound [10] or temporally interfering electric fields [11].

This study evaluates this question. We use defined anatomical landmarks to linearly register the MNI152 brain template to subject-specific MRIs. Besides evaluating the accuracy of this MRI-free method, we also quantify the sensitivity of the method with respect to the number of anatomical landmarks and specific target location.

2. Materials and Methods

2.1. Subjects

Subject data were obtained from six unique data repositories on OpenNeuro.org [12–17]. T1-weighted MRI volumes were manually chosen from studies containing healthy subjects over the age of 18. Subjects with anatomical fiducials redacted or obscured were removed. Fifty subjects in total were analyzed with mean age of 36 ± 18.6 (mean ± sd), 28% female.

2.2. Anatomical fiducial landmarks

Nine anatomical fiducials were identified and marked for all subjects: nasion, left and right inner canthus (LIC and RIC), left and right outer canthus (LOC and ROC), left and right pre-auricular points (LPA and RPA), left and right external meatus (LEM and REM).

All anatomical fiducial markers were identifiable. The 9 unique fiducial markers in this work were selected for their well-defined

* Corresponding author.
E-mail address: tom.riis@utah.edu (T.S. Riis).

https://doi.org/10.1016/j.brs.2024.12.1478
Received 17 September 2024; Received in revised form 8 December 2024; Accepted 31 December 2024
Available online 3 January 2025
1935-861X/© 2025 The Authors. Published by Elsevier Inc. This is an open access article under the CC BY-NC-ND license (http://creativecommons.org/licenses/by-nc-nd/4.0/).

position, enabling accurate and rapid registration. The nasion is the most posterior point at the root of the nose along the midline [18,19]. The naming convention LIC and RIC refers to the left and right medial canthi, proximal to the nose. LOC and ROC refer to the left and right lateral canthi, distal to the nose [20]. The locations of the LPA and RPA are not consistently defined across literature [19,21,22]. In this work, their location is defined as the depression superior to tragus at its base, located on a line connecting the helix to the peak of the tragus. The use and definition of the LEM and REM are based on Wolfsberger et al., defined as the most posterior point of the rim of the posterior wall of the external acoustic meatus, marked as a hyperintense structure on MRI [18]. Example labeling of anatomical fiducial markers is found in Suppl. Fig. 1.

2.3. Registrations

Registration between the MNI152 template brain and subject brain was performed using two transforms: a nonlinear transform based on the extracted brain volume, and a linear transform based on the point matching of anatomical fiducial markers of the face (Fig. 1). The nonlinear transform operates on the brain-extracted volumes of both the subject and template MRI. The brain volume was extracted from the head MRI using command *mri_synthstrip* in Freesurfer [23].

2.3.1. Nonlinear registration

The extracted template brain was first linearly registered (*flirt*, FSL [24]) to subject space and then nonlinearly registered (*fnirt*, FSL) from the previous linear registration to the subject's specific brain morphology. The transforms were saved and then applied to the brain targets in template space (*img2imgcoord*, FSL) to obtain the gold standard registration of deep brain targets in subject space. Nonlinear registration was manually checked for accuracy. Subjects where the transform failed were discarded and replaced.

2.3.2. Anatomical landmark registration

We determined a linear transformation between the MNI152 template brain and the subject brain by point matching of anatomical landmarks on the face. The MATLAB function *absor* [25] provides a least

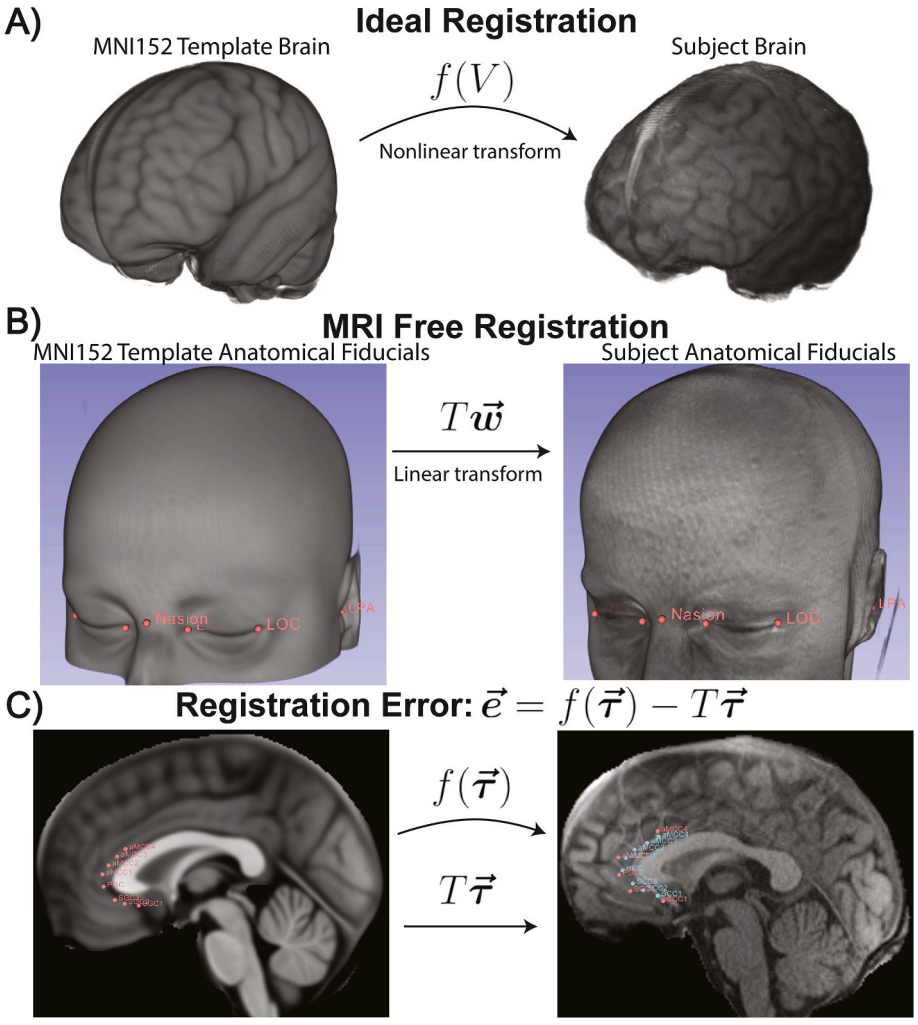

Fig. 1. Experimental Setup.
a, Ideal case: MRI-based nonlinear registration between brain volumes. We employed a nonlinear transformation (*flirt*, FSL [24]), $f(V)$, between the MNI-template and the subject's brain volume. This transformation represents the best possible registration from template space to subject space, using all available information about the two brain volumes. **b, Proposed method: Anatomical landmark-based guidance.** Anatomical landmarks on each subjects' face were identified in both the subject-specific and template MRI images. We optimized a linear transform, T, that minimizes the error between the subject's anatomical landmarks and the template anatomical landmarks (Methods). The hallmark of this method is that it does not require MRI. **c, Evaluation of targeting accuracy**. We calculated the mismatch, e→, between the ideal and the MRI-free registration for targets within the Anterior Cingulate Cortex (ACC) and at anatomical landmarks of Anterior Commissure (AC) and Posterior Commissure (PC).

squares estimation of the rotation, scaling, and translation to minimize the error between the anatomical landmarks in the template space and the corresponding landmarks in the subject space. Specifically, the linear transform was determined by minimizing the equation:

$$J = \mathbf{sR}\vec{w}_{template} + \mathbf{t} - \vec{w}_{subject}$$

where $\vec{w}_{template}$ and $\vec{w}_{subject}$ represent the coordinates of the anatomical landmarks on the template and subject and **s**, **R**, and **t** represent the scaling, rotation, and translation parameters to optimize. Horn's quaternion-based method was used to calculate the transform from anatomical fiducial markers in template space to the matching anatomical fiducials in subject space.

2.4. Calculation of target registration error

2.4.1. Targets

Seven targets in the anterior cingulate cortex (ACC) and two additional targets on the anterior commissure (AC) and posterior commissure (PC) were defined in template space and their coordinates denoted as the vector, $\vec{\tau}$. In the ACC, 3 targets within the subgenual ACC (Brodmann Area 25 [26]) and 4 targets from within the pregenual to anterior mid cingulate cortex (Brodmann Areas s24, p24, a24, 33 [26]) were chosen. Each of the 7 targets was centered on the subject's midline in the x-dimension. Each target was separated from the adjacent target by approximately 5 mm in the sagittal plane (y-z dimension) to provide a continuum spanning the ACC (Fig. 1c). The position of the anterior commissure (AC) and posterior commissure (PC) of the subject's brain was detected using an automatic detection algorithm [27]. Location of the AC and PC were then manually checked for each subject and adjusted as necessary.

2.4.2. Target registration error

The nonlinear transform, *f*, and linear transform, *T*, were applied to the deep brain anatomical targets defined in template space, $\vec{\tau}$. $f(\vec{\tau})$ represents the targets in subject space given the ideal, nonlinear transform with subject-specific MRI. $T\vec{\tau}$ denotes the targets in subject space using the linear transform defined only using anatomical landmarks on the face, without any use of a subject-specific MRI. We calculated the registration error, $\vec{e}$, as the three dimensional difference of these two targeting methods:

$$\vec{e} = f(\vec{\tau}) - T\vec{\tau} \quad (1)$$

2.5. AC-PC coordinate system

All errors were calculated in AC-PC space to compare across subjects. In this coordinate system, the X dimension is the normal vector of the plane along the brain midline, the Y dimension is the vector from posterior commissure (PC) to anterior commissure (AC), and the Z dimension is taken as the cross product of the X and Y vectors with the ventral to dorsal direction positive.

2.6. Data availability

The data associated with the article is available at onetarget.us/download/MRINeuroNavData.

2.7. Code availability

The code associated with the article is available and documented at onetarget.us/download/MRINeuroNav.

3. Results

We have evaluated the guidance accuracy of an MRI-free, facial fiducial landmark-based method, relative to an ideal case in which MRI images of a subject's brain are available (Fig. 1). In this method, a linear transform comprised of scaling, rotation, and translation was optimized to minimize the point matched difference between anatomical fiducials on the template MRI face and the subject MRI face (see Materials and Methods). This transform was then applied to deep brain targets in the template brain to give the locations in subject space. We then compared this MRI-free targeting to the ideal MRI- based targeting. Distances between these two targets were calculated in the X, Y, and Z dimensions in each subject's AC-PC space, with R being the total distance between the two targets (Table 1).

We first asked whether the method is sensitive to the number of fiducial markers defined on a subject's face. Specifically, we measured the target registration accuracy across 9 deep-brain targets for three sets of common anatomical fiducial markers labeled as 3, 5, 9 in Fig. 1a. There was a significant effect of the number of anatomical fiducial markers used for co-registration on the total error across targets ($F_{2,8} = 197.92, p < 0.0001$). Post-hoc analysis shows a significantly larger error encountered using three anatomical fiducial markers compared to five ($p < 0.0001$, two-sample *t*-test; Bonferroni-corrected). Nonetheless, we found no significant difference between using five anatomical fiducial markers and all nine anatomical fiducial markers ($p = 0.52$, two-sample *t*-test; Bonferroni-corrected).

Because using nine fiducial markers conferred no additional benefit over five, we henceforth evaluate accuracy based on the five fiducial markers. The key result—the registration error for each deep brain target—is shown in Fig. 2. Across the targets, this registration method showed an absolute error of 1.11 ± 0.74 *X*, 3.43 ± 2.71 *Y*, 3.59 ± 2.84 *Z*, and 5.75 ± 2.98 *R* total distance (mean ± sdsd). The figure reveals that there is a relatively tight distribution for targets in the subcallosal part of the cingulate cortex (SCC) and a larger variance for targets within the anterior part of the middle cingulate cortex (aMCC). One way ANOVA revealed a significant effect of target ($F_8 = 1.99, p = 0.046$, one-way ANOVA).

These targets showed small average error in the left-right, X dimension (≤ 1.5 mm). This enabled us to visualize the bulk of the targeting error on a single plane along the Y and Z dimensions. To do so, we transformed the ideal, nonlinearly registered targets in subject space into template space using the inverse of the linear transform derived from anatomical fiducials on the face. The X coordinate of the targets in template space was then assigned to the value of the midline, X = 0, to visualize the distribution of linearly registered targets on the same brain in the YZ plane (Fig. 3, Suppl. Fig. 2, Suppl. Fig. 3). This simplified visualization provides the same general insight: A relatively tight distribution for targets within the SCC and larger variance for targets within the aMCC.

The quality of the proposed method rests on the fiducial marker registration accuracy. We therefore evaluated the registration error between anatomical fiducial markers in the subject space and the brain template space. Fig. 4 shows the position error between the registered template anatomical fiducial markers and the fiducial markers on the subject's MRI. The mean ± sd error was 1.80 ± 1.63 mm for *X*, 1.92 ± 1.48 mm for *Y*, 1.08 ± 0.89 mm for *Z*, and 3.25 ± 1.79 mm for *R*. This low error generally denotes a reasonable fit between the subject anatomical fiducials and the registered template anatomical fiducials. Finally, we investigated whether these errors could predict the deep brain target errors. A multiple regression analysis was conducted with the predictors being MNI to subject anatomical fiducial error (at the nasion, LOC, ROC, LPA, and RPA) and the dependent variable being the summed error across the 9 deep brain targets. The regression model explained 17 % of the variance in the summed error ($R^2 = 0.17$, Adjusted $R^2 = 0.0759$), and was statistically insignificant, $F(5,44) = 1.81$, $p = 0.132$ (Table S1, Suppl. Fig. 4).

Table 1
Target registration error across number of anatomical fiducials. Target registration error absolute value for each set of anatomical fiducials (Nasion-LOC- ROC, Nasion-LOC-ROC-LPA-RPA, Nasion-LIC-RIC-LOC-ROC-LPA-RPA-LEM-REM). All values are presented in millimeters (mean ± sd).

Target	Three Anatomical Fiducials				Five Anatomical Fiducials				All Anatomical Fiducials			
	X	*Y*	*Z*	*R*	*X*	*Y*	*Z*	*R*	*X*	*Y*	*Z*	*R*
SGC1	1.34 (0.99)	4.33 (3.7)	6.91 (4.66)	9.22 (4.4)	1.1 (0.7)	3.03 (2.51)	3 (2.69)	5.03 (2.83)	1.15 (0.74)	2.8 (2.19)	2.79 (2.51)	4.7 (2.54)
SGC2	1.25 (0.94)	4.33 (3.64)	6.34 (4.22)	8.77 (3.9)	1.21 (0.65)	3.21 (2.62)	3.05 (2.47)	5.16 (2.77)	1.24 (0.69)	2.94 (2.39)	2.81 (2.36)	4.83 (2.53)
SGC3	1.2 (0.86)	4.4 (3.66)	5.95 (3.95)	8.5 (3.67)	1.2 (0.63)	3.37 (2.65)	3.01 (2.39)	5.22 (2.75)	1.23 (0.67)	3.15 (2.42)	2.81 (2.25)	4.93 (2.5)
PGC	1.15 (0.84)	4.74 (3.85)	5.75 (4.11)	8.56 (3.96)	1.12 (0.7)	3.62 (2.76)	3.23 (2.56)	5.62 (2.79)	1.16 (0.74)	3.42 (2.61)	3.11 (2.24)	5.36 (2.5)
aMCC1	1.15 (0.89)	5.07 (4.18)	6.09 (4.69)	9.12 (4.53)	1.15 (0.72)	3.82 (2.94)	3.76 (2.8)	6.19 (2.92)	1.18 (0.77)	3.63 (2.81)	3.54 (2.54)	5.9 (2.65)
aMCC2	1.16 (0.97)	5.19 (4.45)	6.62 (5.27)	9.72 (5.07)	1.14 (0.76)	3.83 (3.05)	4.1 (3.02)	6.48 (3.1)	1.18 (0.8)	3.64 (2.93)	3.86 (2.74)	6.18 (2.82)
aMCC3	1.23 (1.02)	5.24 (4.58)	7.23 (5.86)	10.27 (5.63)	1.11 (0.82)	3.7 (3.03)	4.42 (3.25)	6.61 (3.32)	1.12 (0.88)	3.62 (2.79)	4.16 (2.99)	6.34 (2.97)
AC	1.65 (1.23)	4.45 (4.02)	8.46 (5.9)	10.69 (5.65)	0.93 (0.75)	2.87 (2.28)	3.82 (2.96)	5.43 (2.92)	0.99 (0.81)	2.54 (1.9)	3.52 (2.73)	4.98 (2.57)
PC	2.06 (1.57)	5.85 (4.75)	10.67 (7.44)	13.38 (7.29)	1.05 (0.89)	3.44 (2.58)	3.95 (3.19)	6 (3.15)	1.12 (0.88)	3.05 (1.96)	3.63 (2.74)	5.43 (2.51)

4. Discussion

In this study, we assessed the guidance accuracy of a neuronavigation method that does not require taking MRI scans. The method leverages anatomical fiducial landmarks measured on each subject's face, and the average MNI152 template head and brain model. The anatomical fiducial markers of the template head were registered to the anatomical fiducial markers of the individual subjects using a linear transformation comprised of scaling, rotation, and translation. The template brain was subjected to the same transformation. We compared this registration method to the ideal case in which a structural MRI image of each subject's brain is available, and therefore, in which the MNI152 brain model can be registered to the ground truth. Across the tested deep brain targets, the MRI-free method, compared to the ideal MRI-based method, incurred an error of 5.75 ± 2.98 mm (mean ± sd) (Fig. 2, Table 1). Therefore, this method may provide a favorable tradeoff between practicality and guidance accuracy for certain types of neuromodulation methods.

The primary advantage of this approach is its accessibility and cost-effectiveness compared to traditional individual MRI-based neuronavigation. By harnessing readily available anatomical landmarks of the face, this technique can potentially expand neuromodulation interventions to populations where MRI acquisition is either too costly, time-consuming, or unavailable.

The average error may be sufficient for certain types of emerging approaches that modulate deep brain targets. Approaches whose focal volume is broader than the about 6 mm error radius are particularly applicable. For instance, deep TMS may access certain deep brain structures, and the volume of deep TMS at depth far exceeds the 6 mm error [9,28]. Electrical currents using temporal interference [11], which can modulate structures deep in the brain, may also benefit from this approach. More focal methods, such as transcranial focused ultrasound [10], may also benefit from this method, depending on the transducer's given focal volume and brain target.

Compared to other template-based registrations, our total error in the deep brain, 5.75 ± 2.98 mm (mean ± sd) with maximal error of 13.12, was slightly larger than those on the scalp—4.69 ± 2.21 with maximal error of 11.53 [6], and 4.79 ± 2.62 with maximal error of 9.62 [7]. This may be due to the increased anatomical variability of structures within the deep brain compared to the dorsolateral prefrontal cortex or the use of fewer anatomical landmarks for registration [7]. The accuracy of the method is inferior to subject-specific MRI-based approaches [4,29], with the error range possibly limiting its application for cases that require high precision. Additionally, previous work shows that different demographic populations require population-specific brain templates [30]. Adapting this method to better match templates to specific subjects may improve accuracy further. This method only considered linear transformations with equally weighted anatomical fiducial markers. Incorporating non-linear transformations based on surface matching or point clouds [3,4,31–33] of the subject's head may further improve the accuracy. The method presented here is also limited in that it relies on localization of facial fiducial markers, which may be a time-consuming and error-prone step [1,2]. However, the anatomical fiducial markers used in this work were chosen based on their well-defined position to maximize speed and accuracy in the point-matching linear registration. While we found that 5 anatomical fiducials were similarly accurate as all 9 pre-specified anatomical fiducial markers in the template matching, adding additional anatomical fiducial markers on the face and scalp [7] would likely improve accuracy. Future work may improve speed and accuracy of registration with models that produce a 3D head surface from optical images taken of the subject's head [33,34], then perform a point cloud registration from the skin surface of the MNI152 MRI to the optically obtained subject-specific 3D head surface. Additionally, future studies would benefit from generalization of the error quantification in targets across the entire brain, rather than just ACC, AC, and PC. Indeed, we observed a significant difference in error based on the target position

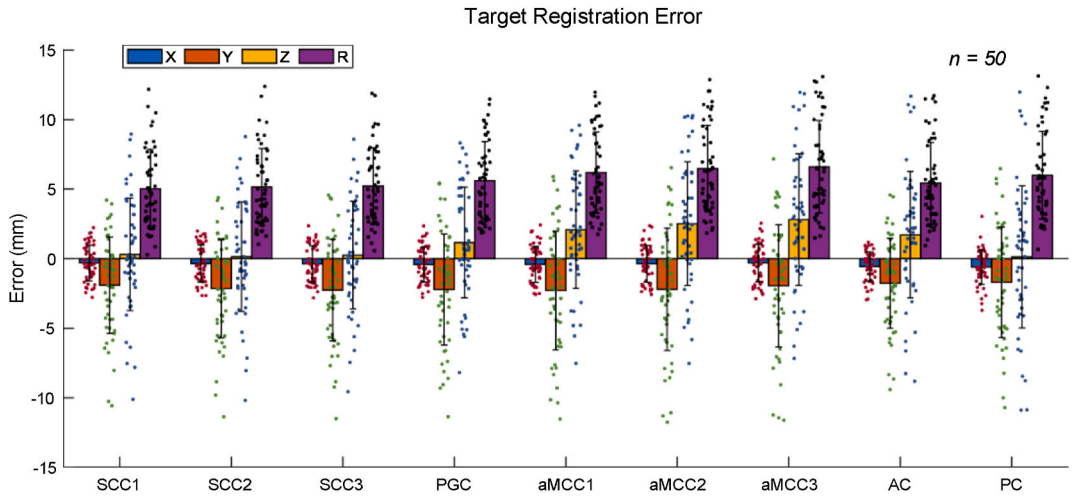

Fig. 2. MRI-free registration compared to the ideal case.
Targeting error between the MRI-free method based on five anatomical fiducial markers (Nasion, Left Outer Canthus, Right Outer Canthus, Left Periaricular Area, Right Periaricular Area) and the ideal, MRI-based nonlinear registration. The X, Y, Z dimensions are the respective dimensions in each subject's AC-PC space, with R being the total distance between the two targets. Error bars show standard deviation.

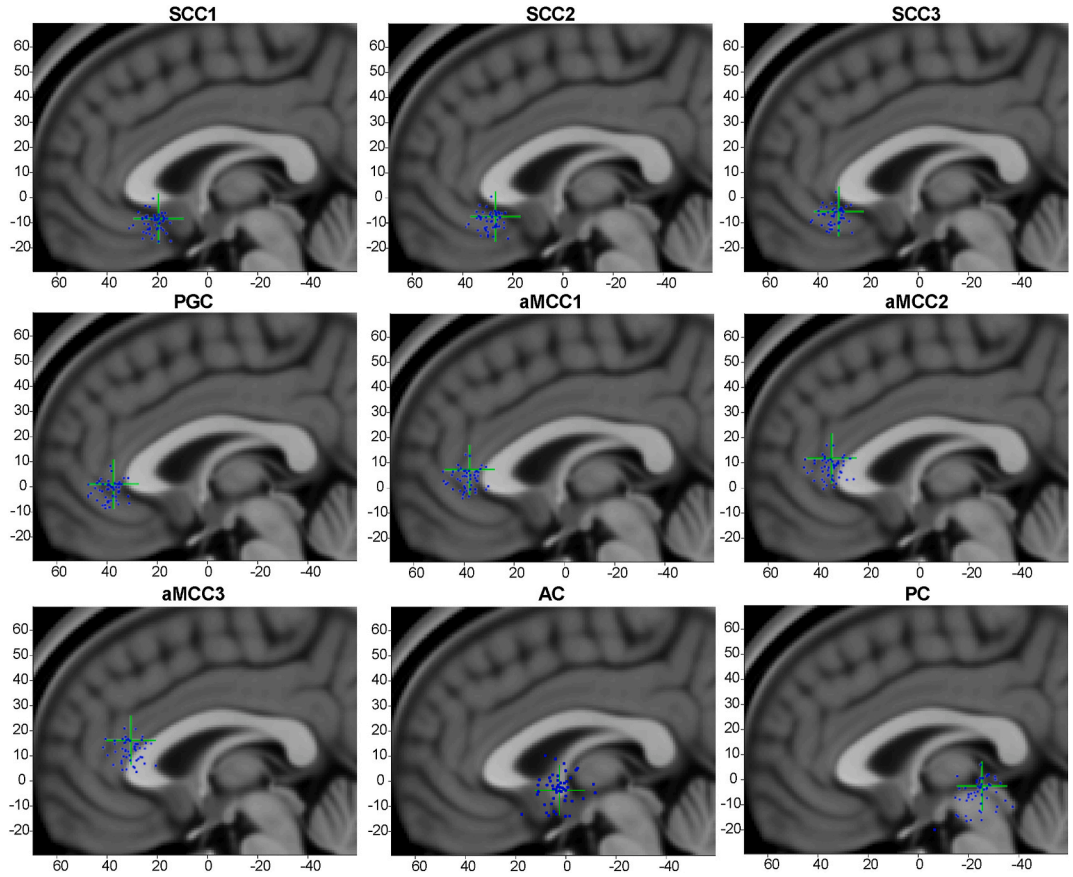

Fig. 3. Sagittal plane distribution of target registration.
Projection of all registered targets on midline and registered to MNI152 template space.

across this small subset of brain targets (Fig. 2, Table 1), suggesting that targeting error is a function of anatomical variability for each region of the brain.

In summary, we show that the knowledge of facial landmarks can provide a neuronavigation method that can target deep brain structures with reasonable accuracy while not requiring the acquisition of MRI scans. This method may increase the practicality and access to certain kinds of neuromodulation techniques.

CRediT authorship contribution statement

Thomas S. Riis: Writing – original draft, Visualization, Validation, Software, Investigation, Formal analysis, Conceptualization. **Seth Lunt:** Writing – review & editing, Validation, Data curation. **Jan Kubanek:** Writing – original draft, Validation, Supervision, Resources, Project administration, Funding acquisition.

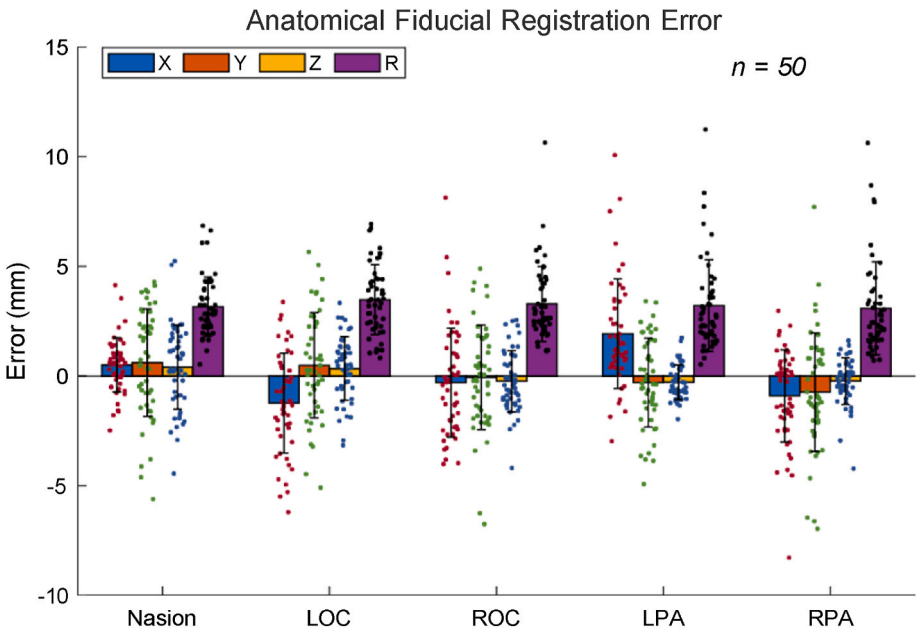

Fig. 4. Anatomical Fiducial Registration Error.
Registration error between subject's anatomical fiducial markers and linearly registered MNI152 template anatomical fiducial markers. Error bars show standard deviation.

Declaration of competing interest

The authors declare the following financial interests/personal relationships which may be considered as potential competing interests: T. S.R. and J.K. have equity/stock options and have received salary and/or consulting fees from SPIRE Therapeutics, Inc.

Acknowledgments

This work was supported by the NIH grants R00NS100986, RF1NS128569, and by grants from the Margolis Foundation, the University of Utah Vice President for Research, the Mildred P. Hunter Foundation, and University of Utah Partners for Innovation, Ventures, Outreach & Technology.

Appendix A. Supplementary data

Supplementary data to this article can be found online at https://doi.org/10.1016/j.brs.2024.12.1478.

References

[1] Thompson EM, Anderson GJ, Roberts CM, Hunt MA, Selden NR. Skull-fixated fiducial markers improve accuracy in staged frameless stereotactic epilepsy surgery in children: clinical article. J Neurosurg Pediatr 2011;7(1):116–9. https://doi.org/10.3171/2010.10.PEDS10352.

[2] Mascott CR, Sol JC, Bousquet P, Lagarrigue J, La- zorthes Y, Lauwers-Cances V. Quantification of true in vivo (ap- plication) accuracy in cranial image-guided surgery: influence of mode of patient registration. Neurosurgery 2006;59(1 SUPPL. 1). https://doi.org/10.1227/01.NEU.0000220089.39533.4E.

[3] Noirhomme Q, Ferrant M, Vandermeeren Y, Olivier E, Macq B, Cuisenaire O. Registration and real-time visualization of transcranial magnetic stimulation with 3-d mr images. IEEE (Inst Electr Electron Eng) Trans Biomed Eng 2004;51:1994–2005. https://doi.org/10.1109/TBME.2004.834266.

[4] Mongen MA, Willems PW. Current accuracy of surface matching compared to adhesive markers in patient-to-image registration. Acta Neurochir 2019:865–870doi. https://doi.org/10.1007/s00701-019-03867-8.

[5] Mazziotta J, Toga A, Evans A, Fox P, Lancaster J, Zilles K, Woods R, Paus T, Simpson G, Pike B, Holmes C, Collins L, Thompson P, MacDonald D, Iacoboni M, Schormann T, Amunts K, Palomero-Gallagher N, Geyer S, Parsons L, Narr K, Kabani N, Le Goualher G, Feidler J, Smith K, Boomsma D, Hulshoff Pol H, Cannon T, Kawashima R, Mazoyer B. A four-dimensional probabilistic atlas of the human brain. J Am Med Inf Assoc : JAMIA 2001;8(5):401–30. https://doi.org/10.1136/jamia.2001.0080401.

[6] Carducci F, Brusco R. Accuracy of an individualized mr-based head model for navigated brain stimulation. Psychiatry Research - Neu- roimaging 2012;203:105–8. https://doi.org/10.1016/j.pscychresns.2011.12.013.

[7] Fleischmann R, Köhn A, Tränkner S, Brandt SA, Schmidt S. Individualized template mri is a valid and reliable alternative to individual mri for spatial tracking in navigated tms studies in healthy subjects. Front Hum Neurosci 2020;14(5). https://doi.org/10.3389/fnhum.2020.00174.

[8] Caulfield KA, Fleischmann HH, Cox CE, Wolf JP, George MS, McTeague LM. Neuronavigation maximizes accuracy and precision in tms positioning: evidence from 11,230 distance, angle, and electric field modeling measurements. Brain Stimul 2022;15:1192–205. https://doi.org/10.1016/j.brs.2022.08.013.

[9] Zibman S, Pell GS, Barnea-Ygael N, Roth Y, Zangen A. Application of transcranial magnetic stimulation for major depression: coil design and neuroanatomical variability considerations. Eur Neuropsychopharmacol 2021;45:73–88. https://doi.org/10.1016/j.euroneuro.2019.06.009. 10.1016/j.euroneuro.2019.06.009.

[10] Lee K, Park TY, Lee W, Kim H. A review of functional neu- romodulation in humans using low-intensity transcranial focused ul- trasound. Biomedical Engineering Letters 2024;14(3):407–38. https://doi.org/10.1007/s13534-024-00369-0. 10.1007/s13534-024-00369-0.

[11] Zhu Z, Yin L. A mini-review: recent advancements in tempo- ral interference stimulation in modulating brain function and behav- ior. Front Hum Neurosci 2023;17(September):1–6. https://doi.org/10.3389/fnhum.2023.1266753.

[12] Kohler PJ, Cottereau BR, Norcia AM. Image segmentation based on relative motion and relative disparity cues in topographically or- ganized Areas of human visual cortex. Sci Rep 2019;9(1):9308. https://doi.org/10.1038/s41598-019-45036-y.

[13] Sunavsky A, Poppenk J. Neuroimaging predictors of cre- ativity in healthy adults. Neuroimage 2020;206:116292. https://doi.org/10.1016/j.neuroimage.2019.116292. URL, https://www.sciencedirect.com/science/article/pii/S1053811919308833.

[14] Ponticorvo S, Esposito F. Hearing loss connectome. 2024. https://doi.org/10.18112/openneuro.ds005026.v1.0.0.

[15] Epp S, Castrillon G, Yuan B, Andrews-Hanna J, Preibisch C, Riedl V. Two distinct modes of hemodynamic responses in the human brain. OpenNeuro. [Dataset] 2023. https://doi.org/10.18112/openneuro.ds004873.v1.0.2.

[16] Horta M, Polk R, Ebner NC. Single dose intranasal oxytocin admin- istration: data from healthy younger and older adults. Data Brief 2023;51:109669. https://doi.org/10.1016/j.dib.2023.109669.

[17] Pereira M, Faivre N, Iturrate I, Wirthlin M, Serafini L, Mar- tin S, Desvachez A, Blanke O, de Ville DV, del JR. Milla'n, Dis- entangling the origins of confidence in speeded perceptual judgments through multimodal imaging. Proc Natl Acad Sci USA 2020;117(15):8382–90. https://doi.org/10.1073/pnas.1918335117.

[18] Wolfsberger S, Roessler K, Regatschnig R, Ungersböck K. Anatomi- cal landmarks for image registration in frameless stereotactic neuronav- igation. Neurosurg Rev 2002;25:68–72. https://doi.org/10.1007/s10143-001-0201-x.

[19] Tsuzuki D, Watanabe H, Dan I, Taga G. MinR 10/20 system: quanti- tative and reproducible cranial landmark setting method for MRI based on minimum initial reference points. J Neurosci Methods 2016;264:86–93. https://doi.org/10.1016/j.jneumeth.2016.02.024.

[20] Pfisterer WK, Papadopoulos S, Drumm DA, Smith K, Preul MC. Fiducial versus nonfiducial neuronavigation registration assessment and considerations of

accuracy. Neurosurgery 2008;62(3 Suppl 1):201–7. https://doi.org/10.1227/01.neu.0000317394.14303.99. ; discussion 207–208.
[21] Prabhu P, Kotegar KA, Mariyappa N, H A, Bhargava GK, Saini J, Sinha S. A novel approach to detect anatomical landmarks using R-CNN for MEG-MRI registration. SSRN Electron J 2022. https://doi.org/10.2139/ssrn.4139903. URL, https://www.ssrn.com/abstract=4139903.
[22] Jasper HH. Report of the committee on methods of clinical exami- nation in electroencephalography: 1957. Electroencephalogr Clin Neurophysiol 1958;10(2):370–5. https://doi.org/10.1016/0013-4694(58)90053-1. URL, https://www.sciencedirect.com/science/article/pii/0013469458900531.
[23] Fischl B, Salat DH, Busa E, Albert M, Dieterich M, Haselgrove C, van der Kouwe A, Killiany R, Kennedy D, Klaveness S, Montillo A, Makris N, Rosen B, Dale AM. Whole brain segmentation. Neuron 2002;33(3):341–55.
[24] Smith SM, Jenkinson M, Woolrich MW, Beckmann CF, Behrens TE, Johansen-Berg H, Bannister PR, De Luca M, Drobnjak I, Flitney DE, Niazy RK, Saunders J, Vickers J, Zhang Y, De Stefano N, Brady JM, Matthews PM. Advances in functional and structural mr image analysis and implementation as fsl. Neuroimage 2004;23. https://doi.org/10.1016/j.neuroimage.2004.07.051. S208–S219, mathematics in Brain Imaging URL, https://www.sciencedirect.com/science/article/pii/S1053811904003933.
[25] Jacobson M. Absolute orientation. 2021. https://www.mathworks.com/matlabcentral/fileexchange/26186-absolute-orientation-horn-s-method?s_tid=ta_fx_results. Online3122024.
[26] Vogt BA. Chapter 1 - the cingulate cortex in neurologic dis- eases: history, Structure, Overview. In: Vogt BA, editor. Hand- book of clinical neurology, vol. 166. Elsevier; 2019. p. 3–21. https://doi.org/10.1016/B978-0-444-64196-0.00001-7. URL, https://www.sciencedirect.com/science/article/pii/B9780444641960000017.
[27] Ardekani BA, Bachman AH. Model-based automatic detection of the anterior and posterior commissures on MRI scans. Neuroimage 2009;46(3):677–82. https://doi.org/10.1016/j.neuroimage.2009.02.030.
[28] Tendler A, Goerigk S, Zibman S, Ouaknine S, Harmelech T, Pell GS, Zangen A, Harvey SA, Grammer G, Stehberg J, Adefolarin O, Muir O, MacMillan C, Ghelber D, Duffy W, Ma- nia I, Faruqui Z, Munasifi F, Antin T, Padberg F, Roth Y. Deep TMS H1 Coil treatment for depression: results from a large post marketing data analysis. Psychiatr Res 2023;324(March). https://doi.org/10.1016/j.psychres.2023.115179.
[29] Liu W, Ding H, Han H, Xue Q, Sun Z, Wang G. The study of fiducial localization error of image in point-based registration. Pro- ceedings of the 31st annual international conference of the IEEE engineering in medicine and biology society: engineering the fu- ture of biomedicine, EMBC 2009 (september). 2009. p. 5088–91. https://doi.org/10.1109/IEMBS.2009.5332731.
[30] Tang Y, Hojatkashani C, Dinov ID, Sun B, Fan L, Lin X, Qi H, Hua X, Liu S, Toga AW. The construction of a Chinese mri brain atlas: a morphometric comparison study be- tween Chinese and caucasian cohorts. Neuroimage 2010;51:33–41. https://doi.org/10.1016/j.neuroimage.2010.01.111.
[31] Vema Krishna Murthy S, MacLellan M, Beyea S, Bardouille T. Faster and improved 3-D head digitization in MEG using Kinect. Front Neurosci 2014;8:326. https://doi.org/10.3389/fnins.2014.00326. URL, https://pubmed.ncbi.nlm.nih.gov/25389382. http://www.ncbi.nlm.nih.gov/pmc/articles/PMC4211394.
[32] Zetter R, Iivanainen J, Parkkonen L. Optical Co-registration of MRI and on-scalp MEG. Sci Rep 2019;9(1):5490. https://doi.org/10.1038/s41598-019-41763-4.
[33] Fan Y, Jiang D, Wang M, Song Z. A new markerless patient-to- image registration method using a portable 3D scanner. Med Phys 2014;41(10). https://doi.org/10.1118/1.4895847.
[34] Hou Y, Ma L, Zhu R, Chen X, Zhang J. A low-cost iphone-assisted augmented reality solution for the localization of intracranial lesions. 2016. https://doi.org/10.1371/journal.pone.0159185.